Diurnal and semi-diurnal tidal structures due to O_2, O_3 and H_2O heating

Geeta Vichare* and R Rajaram

Indian Institute of Geomagnetism, New Panvel, Navi Mumbai 410 218, India.
**Corresponding author. e-mail: vicharegeeta@gmail.com*

Today with increased availability of data of middle atmospheric winds and temperature, modelling of middle atmospheric tides has acquired greater importance. The theory of atmospheric tides has two main parts: (i) Investigation of the sources of periodic excitation, and (ii) calculation of the atmospheric response to the excitation. Other than stratospheric ozone and tropospheric water vapour absorption, the thermal energy available from the absorption in Schumann–Runge (SR) continuum leading to photo-dissociation of O_2 is important energy source for tides in the lower thermosphere. PHODIS radiative transfer model is capable of providing tidal forcing due to combined effect of solar and chemical heating in the wavelength region 116 to 850 nm. In this paper, we present an atmospheric tidal model based on classical tidal theory and the prime objective is to obtain the tidal structure due to conventional ozone and water vapour heating in conjunction with the O_2 absorption. Mean wind and dissipation mechanisms are not considered. The present tidal model reveals that the diurnal amplitude peaks in mid to low latitudes, whereas semidiurnal component is stronger at higher latitudes. The semidiurnal tide is about an order of magnitude weaker than the diurnal tide. Also, semidiurnal wave has longer vertical wavelength than diurnal tide. The results of present model are qualitatively in good agreement with the other tidal models, which utilize more sophisticated parameterization. Thus, the salient features of the tidal structure are obtained using basic computations without considering the effects of background winds and dissipation processes. Further refinements to the model can serve as an inexpensive substitute to the presently available tidal models.

1. Introduction

The Earth's atmosphere responds to gravitational and thermal forces in a manner analogous to forced mechanical vibrations. The thermally forced atmospheric tides are excited by the periodic absorption of solar radiation connected with the apparent sidereal motion of the Sun around the Earth. Characteristics of the diurnal and semi-diurnal components of the tidal oscillations have been studied extensively using various techniques such as rocket sounding, radar, lidar measurements and space-based observations (Vincent 1984; Sasi and Krishna Murthy 1990; Deng *et al.* 1997; Rajaram and Gurubaran 1998; Vincent *et al.* 1998; Tsuda *et al.* 1999; Ratnam *et al.* 2002; Pancheva *et al.* 2003; Riggin *et al.* 2003; Xu *et al.* 2009; Zhao *et al.* 2012). Also, number of attempts has been made towards the modelling of tides (Forbes 1982; Lieberman and Leovy 1995; Miyahara and Miyoshi 1997; Wood and Andrews 1997; Hagan and Forbes 2002, 2003; Grieger *et al.* 2002; Zhang *et al.* 2010).

The theory of atmospheric tides has two main parts: (i) Investigation of the sources of periodic

Keywords. Atmospheric tides; atmospheric tidal model; Phodis heating; O_2, O_3 and H_2O heating; diurnal tide; semi-diurnal tide.

excitation, and (ii) calculation of the atmospheric response to the excitation. Therefore, in order to numerically simulate the Earth's upper atmospheric circulation, the accurate knowledge of the heat budget of the atmosphere is essential. During photo-dissociation of the absorbing species, substantial portions of the incident energy may appear as internal energy of the excited species or as chemical potential energy of the product species. Thus the absorbed solar energy does not all immediately appear as heat, rather heating is a multistep process, which makes the accurate evaluation of the heating rates of the atmosphere more complicated. Moreover, absorption in the atmosphere takes place by various atoms and molecules such as O_2, O_3, H_2O, N_2, N, CO_2, etc. However, considering all of them together affects the clarity in arriving at the cause and effect discussions. The main absorbing molecules responsible for thermal tides are O_3 in the stratosphere and mesosphere (Butler and Small 1963), H_2O in the troposphere (Siebert 1961) and O_2 in the thermosphere. Extensive work has been performed for first two components (Chapman and Lindzen 1970; Forbes and Garrett 1978; Groves 1982; Groves and Wilson 1982), whereas fewer efforts have been made for the forcing due to oxygen molecule. The O_2 heating is significant in the thermosphere and it is found that the heating in the Schumann–Runge (SR) bands is the dominant heat source between 88 and 96 km, while absorption in the SR continuum is most important above 96 km (Strobel 1978). Therefore, it is vital to simulate the atmospheric tides for oxygen heating too. In this paper we present modelling results of diurnal and semidiurnal tides in the atmosphere due to O_3, H_2O and O_2 heating using classical tidal theory. Here we demonstrate that the simple computations of the tides without considering the mean wind and dissipation mechanisms can also reproduce the broad features of the atmospheric tides, and is qualitatively in good agreement with the other existing sophisticated tidal models. The aim of the present paper is to introduce our atmospheric tidal model. For the present tidal model, we use PHODIS radiative transfer model to reproduce the heating due to stratospheric ozone and lower thermospheric oxygen absorption, which is discussed in section 2. The tropospheric water vapour heating is computed separately using the well-established Grove's method (Groves 1982). The mathematical description of the model is presented in section 3. The height profiles of the Hough components of diurnal and semi-diurnal waves have been discussed in section 4. Thus, sections 2 and 4 take care of the sources of periodic excitation and section 3 describes the computation of the atmospheric response to the excitation. The tidal perturbations in neutral wind derived from present model simulations are discussed in section 5. Scope of the future work is outlined in section 6, and the last section presents the summary.

2. Heating rates obtained from 'PHODIS'

The solar ultraviolet radiation absorbed by ozone and molecular oxygen in the mesosphere and lower thermosphere produces heating through a series of complex processes and it is strongly dependent on wavelength of impinging solar radiation. Ozone is the main absorber of wavelength ∼240–320 nm, O_2 of ∼100–200 nm, and both O_3 and O_2 absorb radiation of wavelength ∼200–240 nm. Absorption below ∼100 nm can occur by various other molecules and atoms, such as N_2, O_2, N, O.

PHODIS is a software package developed by Arve Kylling (Kylling *et al.* 1995), to calculate photo dissociation rates for number of molecules such as O_2, O_3, NO_2, CO_2 and also computes the heating rate due to O_3 and O_2 absorption in the wavelength region 116 to 850 nm. Many atmospheric models such as Finish Meteorological Institute's FinROSE chemistry transport model (FinROSE-ctm) (Damski *et al.* 2007), the EMEP Eulerian photochemistry model (Simpson *et al.* 2012), etc., use photodissociation coefficients compiled by PHODIS radiative transfer model. Simpson *et al.* (2002) compared the PHODIS photolysis rate coefficients of NO_2 with observations and found the agreement is good under clear sky conditions.

In PHODIS model, the radiative transfer calculation is divided into three distinct regions: (a) 116.3–177.5 nm (SR Continuum), (b) 177.5–202.5 nm (SR Bands), which uses Minschwaner *et al.* (1993) parameterization, and (c) 202.5–850.0 nm. First two regions employ no multiple scattering (Beer–Lambert law), whereas multiple scattering is included in the third region. All three regions take into account the ozone and molecular oxygen absorption and Rayleigh scattering. To handle multiple scattering in the 202.5–850.0 nm region PHODIS provides an option of three different radiative transfer solvers: (1) The general purpose discrete ordinate algorithm DISORT with plane parallel geometry (Stamnes *et al.* 1988), (2) spherical and pseudo-spherical version of DISORT (Dahlback and Stamnes 1991), and (3) two-stream algorithm (Twostr) (Kylling *et al.* 1995). In the present work, we used first solver (DISORT) to calculate the radiation field in a model atmosphere.

For the present simulations, we have used a tropical (15°N) atmosphere as a background

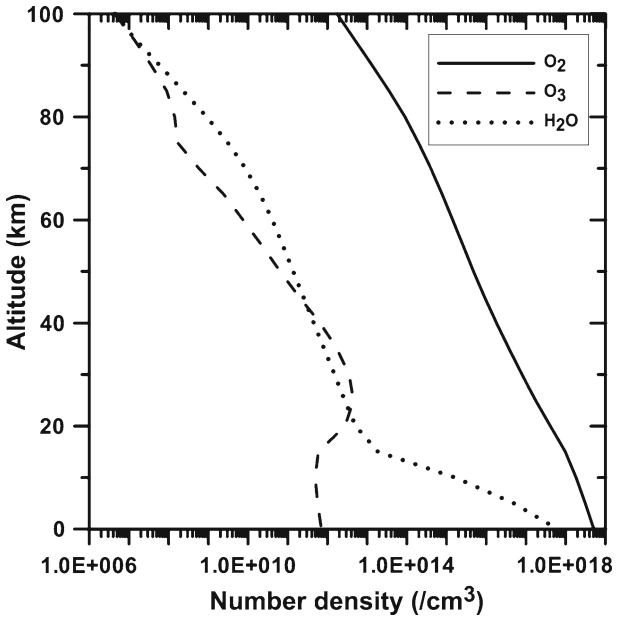

Figure 1. Height profile of neutral densities.

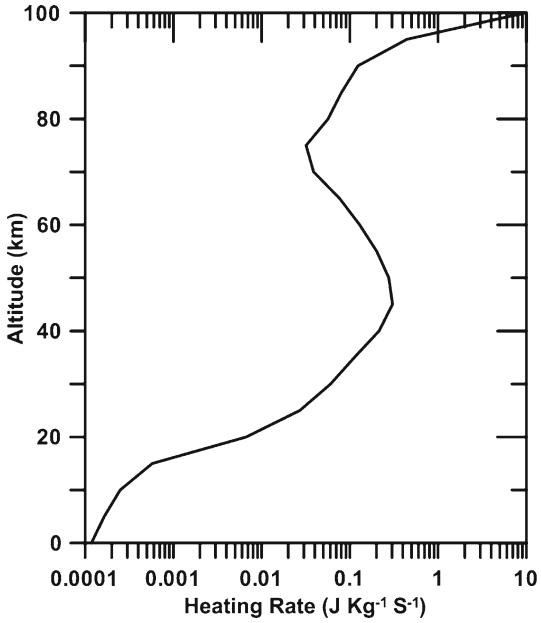

Figure 2. Height profile of heating rates obtained from PHODIS during equinox at noon, at geographic equator.

atmosphere, which is based on the Air Force Geophysics Laboratory's (AFGL) Atmospheric Constituent Profiles model (Anderson *et al.* 1986). In this model, the vertical structure including temperature, pressure and density distributions, plus mixing ratio profiles of H_2O, CO_2, O_3, N_2O, CO, and CH_4, were initially taken from U.S. Standard Atmosphere. Altogether, vertical profiles of the number densities of 28 constituents (H_2O, CO_2, O_3, N_2O, CO, CH_4, O_2, NO, SO_2, NO_2, HNO_3, OH, HF, HCl , HBr, HI, ClO, OCS, H_2CO, HOCl, N_2, HCN, CH3Cl , H_2O_2, C_2H_2, C_2H_6, and PH_3) are provided by the model. The height profiles of number densities of O_2, O_3 and H_2O at the tropical region are depicted in figure 1.

The PHODIS package also provides the facility to include water clouds, cirrus clouds, background aerosols, and different albedoes too. Temperature, pressure and ozone profiles are required to evaluate the optical properties of the atmosphere such as optical depth, phase function and single scattering albedo (which is the ratio of optical depth of scattering to total optical depth). The extra-terrestrial solar flux data used in PHODIS are from World Meteorological Organization (WMO 1986), while the Rayleigh scattering cross section was calculated using the formula of Nicolet (1984). The temperature dependent ozone absorption and scattering cross sections are taken from Molina and Molina (1986), while the parameterization due to Minschwaner *et al.* (1993) is used for molecular oxygen. Cross sections for the various photodissociation rates are mostly taken from DeMore *et al.* (1992). All calculations are performed on the wavelength grid specified by WMO (1986). Higher resolution of 1 nm is used between wavelength 300 and 315 nm.

Figure 2 represents typical heating rates obtained from PHODIS at spring equinox, at the geographic equator during noontime. The mesospheric heating, essentially due to Ozone absorption peaks at around 45 km above the Earth's surface. Whereas, in the lower thermosphere, the heating increases considerably due to molecular oxygen absorption, which normally maximizes around 140 km. Currently used PHODIS code does not include the water vapour heating and hence we compute H_2O vapour heating using Grove's method (Groves 1982). The maximum heating due to insolation absorption by H_2O takes place within first 10 km altitude and is smaller than mesospheric heating by an order of two (not shown here). Though it is known that the clouds (Groves 1982) or airglow phenomenon (Mlynczak and Solomon 1993) can alter the efficiency of solar heating, for simplicity we restrict ourselves to non-cloudy conditions.

3. Model description

Fluctuations associated with tidal oscillations are perturbations in the ambient atmosphere and the entire problem is tackled through linearization $\rho = \rho_0 + \delta\rho$, where ρ_0 is ambient state and $\delta\rho$ is a perturbation. Vertical velocity (w) is assumed to be small compared to horizontal velocities, but dw/dz cannot be ignored.

In tidal theory, generally the fields of concern are periodic in time (t) and longitude (φ)

$$\therefore \quad \text{field} = f_e^{\sigma,s}(\theta, \mathrm{Z})\, e^{i(\sigma t + s\phi)}$$

where θ is colatitudes; $2\pi/\sigma$ = solar or lunar (s/l) day or its suitable fraction.

$$s = 0,\ \pm 1,\ \pm 2,\ \pm 3,\ ....$$

Let $f = \sigma/2\omega$ (ω = Earth's rotation rate)

$$\sigma = \frac{2\pi}{(\text{fraction of } s/l \text{ day}) \cdot (s/l \text{ day})}$$

$$\therefore \quad f = \frac{1}{2\,(\text{fraction of } s/l \text{ day})}.$$

For diurnal wave, $f = 0.5$; for semidiurnal wave, $f = 1$; for two-day wave, $f = 0.25$ and so on.

Equations of momentum, continuity and thermodynamic energy in the atmosphere obeying perfect gas law and hydrostatic pressure equilibrium gives

$$H\frac{\partial^2 G^{\sigma,s}}{\partial Z^2} + \left(\frac{dH}{dZ} - 1\right)\frac{\partial G^{\sigma,s}}{\partial Z} = \frac{g}{4a^2\omega^2} F\left(\left(\frac{dH}{dZ} + \kappa\right) G^{\sigma,s} - \frac{\kappa\, J^{\sigma,s}}{\gamma\, gH}\right) \quad (1)$$

$$F = \frac{d}{d\mu}\left(\frac{1-\mu^2}{f^2-\mu^2}\frac{d}{d\mu}\right) - \frac{1}{f^2-\mu^2}\left(\frac{s}{f}\frac{f^2+\mu^2}{f^2-\mu^2} + \frac{s^2}{1-\mu^2}\right) \quad (2)$$

where $H = (RT_0/g)$; R is gas constant, g is gravity, and T_0 is basic temperature distribution;

$$G = -\frac{1}{\gamma\, P_0}\frac{dP}{dt};$$

P = pressure; P_0 = background atmospheric pressure;

$$\gamma = \frac{Cp}{Cv} = 1.4; \quad \kappa = \frac{\gamma\ -1}{\gamma} = \frac{2}{7},$$

and

$$\mu = \cos\theta.$$

Equation (1) can be solved by the method of separation of variables. Assume that $G^{\sigma,s}$ may be written as:

$$G^{\sigma,s} = \sum_n L_n^{\sigma,s}(\mathrm{Z})\,\Theta_n^{\sigma,s}(\theta) \quad (3)$$

and

$$J^{\sigma,s} = \sum_n J_n^{\sigma,s}(Z)\Theta_n^{\sigma,s}(\theta) \quad (4)$$

where the set $\{\Theta_n^{\sigma,s}(\theta)\}$ for all n is complete for $0 \le \theta \le \pi$.

Substituting (3) and (4) in (1), we get

$$\therefore \quad F(\Theta_n^{\sigma,s}) = -\frac{4a^2\omega^2}{gh_n^{\sigma,s}}\Theta_n^{\sigma,s} \quad (5)$$

and

$$H\frac{d^2 L_n^{\sigma,s}}{dZ^2} + \left(\frac{dH}{dZ} - 1\right)\frac{dL_n^{\sigma,s}}{dZ} + \frac{1}{h_n^{\sigma,s}}\left(\frac{dH}{dZ} + \kappa\right) L_n^{\sigma,s} = \frac{\kappa}{\gamma\, gH h_n^{\sigma,s}} J_n^{\sigma,s} \quad (6)$$

where $h_n^{\sigma,s}$ is a constant of separation.

The boundary conditions on $\{\Theta_n\}$ are that they be bounded at the poles (at $\theta = 0,\ \pi$). With these conditions, equation (5) defines an eigenvalue problem where $\{h_n\}$ is the set of eigenvalues, often called as set of equivalent depths and the eigenfunctions $\{\Theta_n\}$ are called as Hough functions. Equation (6) is a 'Vertical structure equation', and equation (5) is called as 'Laplace's Tidal equation'. The solution of these equations are obtained by the method described in Chapman and Lindzen (1970) and Jadhav (2002). One can calculate the tidal perturbations in zonal (v), meridional (u), and vertical (w) components of wind using following expressions,

$$u = \sum_n u_n(x)\, U_n(\theta) \quad (7)$$

$$v = \sum_n v_n(x)\, V_n(\theta) \quad (8)$$

$$w = \sum_n w_n(x)\, \Theta_n(\theta) \quad (9)$$

where,

$$\begin{aligned}
x &= -\log\left(\frac{P_0}{P_0(0)}\right)\\
U_n &= \frac{1}{f^2 - \cos^2\theta}\left(\frac{d}{d\theta} + \frac{s\cot\theta}{f}\right)\Theta_n\\
V_n &= \frac{1}{f^2 - \cos^2\theta}\left(\frac{\cos\theta}{f}\frac{d}{d\theta} + \frac{s}{\sin\theta}\right)\Theta_n\\
u_n &= \frac{\gamma\, gh_n e^{x/2}}{4a\omega^2}\left(\frac{dy_n}{dx} - \frac{1}{2}y_n\right)\\
v_n &= \frac{i\gamma\, gh_n e^{x/2}}{4a\omega^2}\left(\frac{dy_n}{dx} - \frac{1}{2}y_n\right)\\
w_n &= -\frac{i\sigma}{g}\Omega_n + \gamma\, h_n e^{x/2}\left[\frac{dy_n}{dx} + \left(\frac{H}{h_n} - \frac{1}{2}\right)y_n\right]\\
y_n &= L_n e^{-x/2}.
\end{aligned} \quad (10)$$

Thus, present model solves the linearized and extended classical fluid dynamical equation, for

steady state global wind perturbations. The method of separation of variables is used to solve this equation for latitudinal and vertical variations independently. The latitudinal variation can be obtained through the solution of Laplace's tidal equation expressed in terms of associated Legendre function leading to a third order recurrence relation between the series coefficients (Hough function). The tidal perturbations are computed by considering various Hough modes of heating $\left(J^s_{m,n}\right)$ due to ozone, oxygen and water vapour. The details of the computation of $J^s_{m,n}$ are given in next section. It should be noted that the present model does not account for background winds and for various dissipative forces due to turbulence, molecular diffusion of heat and momentum, infrared cooling, ion drag, etc.

4. Determination of $J^s_{m,n}$

If infinitesimal amount of heat δQ is added per unit mass of air in infinitesimal time δt then,

$$\delta Q = J\delta t \tag{11}$$

where $J = J(z, \theta, \phi, t)$ is the heating rate. Here z indicates height and t is the time. Geographic latitude and longitude are denoted by θ and ϕ, respectively.

Since no explicit function is known for J, it may be expanded as a series,

$$J = \sum_n J_n(z, \theta) e^{i(\sigma t + s\phi)} \tag{12}$$

zonal wavenumber, s, is a positive integer. Chapman and Lindzen (1970) assumed that the variables of $J_n(z, \theta)$ are separable.

Equation (12) can be expressed in terms of Hough functions, $\Theta^s_{m,n}$ as follows:

$$J = \sum_{s,m} \sum_n J^s_{m,n} \Theta^s_{m,n}(\mu)\, e^{i(s\phi + mt)} \tag{13}$$

where μ is a cosine of latitude. This generates $J^s_{m,n}$ as:

$$J^s_{m,n} = e^{i(\text{phase})} \int_0^\pi J_a(\theta)\, \Theta^s_{m,n}(\theta) \sin\theta\, d\theta. \tag{14}$$

Thus, to determine $J^s_{m,n}(z)$, it is necessary to have heating rate as a function of local time, latitude and height, which is obtained from PHODIS. Then at various altitudes and latitudes, the heating rates are expanded in a series of Fourier harmonics of periods 24, 12, 8 hr, etc. At each height, the latitude distribution of each Fourier coefficient is decomposed into Hough modes. In this manner, for each Hough mode, the heating rate can be obtained as a function of latitude and height.

Vertical structures of the Hough components of O_3, O_2 and H_2O heating for diurnal and semi-diurnal modes at the vernal equinox are demonstrated in figures 3 and 4, respectively. In this paper, we present simulation results during spring equinox, when one can expect simpler global picture due to hemispheric symmetry. The bottom side X-axis indicates scale for water vapour heating rate, whereas top side X-axis indicates O_3 and

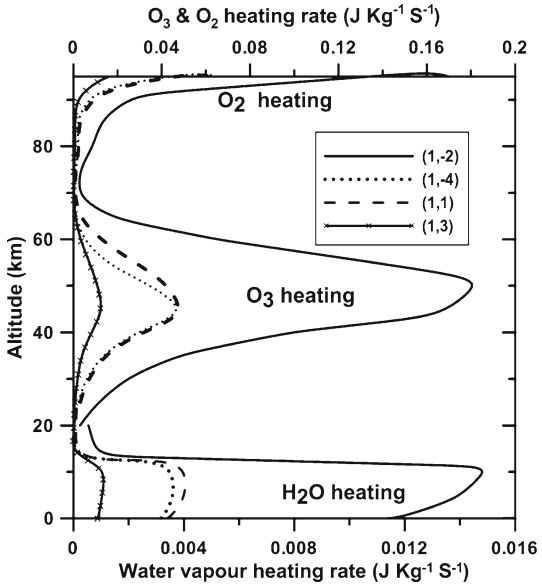

Figure 3. Diurnal heating rate during equinox, due to O_3, O_2 and H_2O vapour absorption, decomposed into Hough functions.

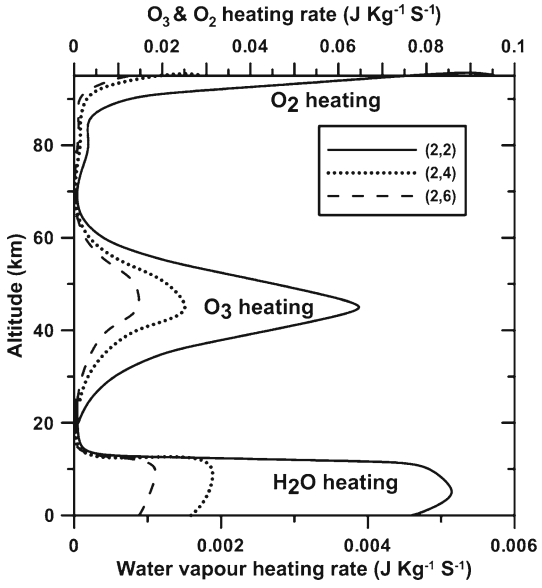

Figure 4. Same as figure 3, but for semi-diurnal component.

O_2 heating rates. The figures show that the vertical heating structure varies between different Hough modes of the same period, while Chapman and Lindzen (1970) had ignored these differences. It is seen from figure 3 that the major heating is associated with (1, −2) mode and next higher contribution comes from (1, 1) and (1, −4) modes in the diurnal component. Since (1, −2) is 'symmetric trapped diurnal mode', it cannot propagate upward and hence do not have much significance in the dynamics of upper thermosphere. While (1, 1) is a 'symmetric propagating diurnal mode', so can play significant role in the upper atmospheric electrodynamics. Three symmetric Hough components of heating for the semi-diurnal tide shown in figure 4 depicts that the (2, 2) mode is dominant.

For water vapour, maximum heating takes place at around 10 km of altitude, whereas mesospheric ozone heating maximizes near 45 km, although the height of maximum concentration of Ozone lies between 20 and 25 km. The diurnal component of heating at the height of 95 km is comparable with that at the mesosphere, whereas semi-diurnal component is higher in the lower thermosphere. The ratios of diurnal peak heating amplitudes (1, −2):(1, 1):(1, 3) for mesospheric O_3 heating are 1:0.25:0.07 and for H_2O heating are 1:0.27:0.07. In the case of semi-diurnal tidal motions, the ratios of (2, 2):(2, 4):(2, 6) for O_3 heating in the mesosphere are 1:0.4:0.23 and for tropospheric H_2O heating are 1:0.36:0.21.

5. Model results

Using equations (7), (8) and (9), the northerly (u), westerly (v) and upward (w) velocities have been computed for diurnal and semi-diurnal components, during vernal equinox. Past observation-based studies have often shown complicated tidal response on autumnal equinox and solstice seasons. Therefore, we present simulations during spring equinox. Figure 5(a) illustrates the simulated altitude structure of the diurnal component of meridional wind at various latitudes, while figure 5(b) shows the phase (hour of maximum). The diurnal component includes (1, −2), (1, 1), (1, −4), (1, 3) and (1, 5) modes of the diurnal variations. Figure 6(a) and (b) present amplitude and hour of maximum of the semidiurnal component of the meridional wind, respectively. This considers symmetric modes of semi-diurnal variations, viz., (2, 2), (2, 4), and (2, 6). The equatorial standard temperature profile is used for the computation of both the components.

Figure 5(a) exhibits the exponential growth of diurnal amplitude with altitude, at low to mid latitudes. At high latitudes, the diurnal amplitude decreases with altitude due to the dominance of trapped modes. Whereas at lower latitudes, the increase of tidal amplitude with lesser neutral density at higher altitudes is due to freely propagating modes. The magnitude of semi-diurnal tide is almost one order smaller than the diurnal tide.

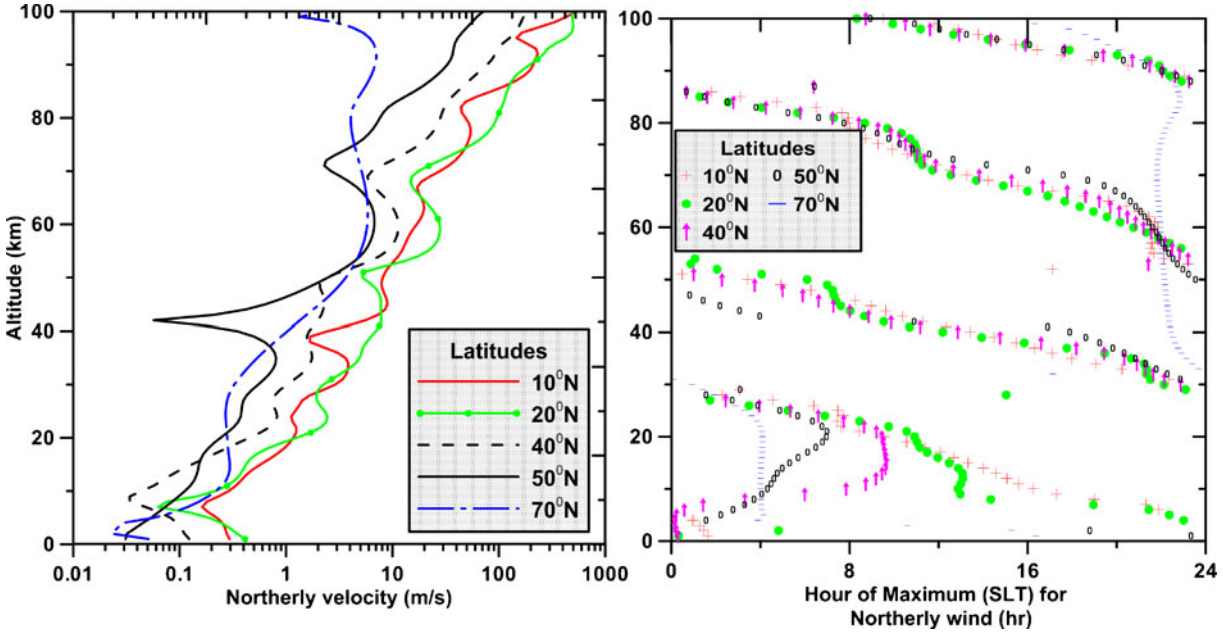

Figure 5. (**a**) Amplitude and (**b**) phase (hour of maximum) of the solar diurnal variation of the meridional wind component, u, at various latitudes.

Semi-diurnal component of the meridional wind in general show increase in magnitude with the altitude, at almost all latitudes (figure 6a). However, near 20 km altitude, the magnitude is minimum for all latitudes, and then it once again drops to lower value at the altitude around 70 km at higher latitudes. In the lower thermosphere, semi-diurnal tide attains almost same amplitudes at all latitudes (within one order difference), while magnitudes of the diurnal tidal component differ by more than one order between high and low latitudes at 100 km altitude. The comparison of present profiles with those obtained by Chapman and Lindzen (1970), in general reveals a very good match. The profiles of diurnal component of meridional wind match very well, especially at lower heights and higher latitudes. The amplitudes at higher altitudes of lower latitudes are higher in the present simulations. The drop in amplitude of semi-diurnal meridional wind near 20 km is also obtained by Chapman and Lindzen (1970). However, the second decrease at around 70 km for higher latitudes was not evident in their profile. The sudden phase change near 20 km is also consistent with those of Chapman and Lindzen (1970). The present height profiles also match with those obtained by Reed *et al.* (1969). The discrepancies at higher altitudes could be largely due to consideration of additional heating source of molecular oxygen.

Here we would like to draw attention to the results obtained by Hagan (1996) using Global Scale Wave Model (GSWM), which also includes oxygen heating. The parameterization used by her for oxygen heating was based on Strobel (1978), whereas PHODIS uses Minschwaner *et al.* (1993) parameterization. Moreover, Hagan (1996) took into account the atmospheric dissipation, which restrains the amplitude of the tidal wind. In spite of these differences, the altitude profiles of the diurnal component of the meridional wind at low latitudes derived using our model are almost similar to that obtained by Hagan (1996), except the magnitudes of the wind. Our model predicts higher values than GSWM. These quantitative differences can be attributed to the non-consideration of dissipation mechanism and background wind.

The distributions of diurnal component of zonal (left) and meridional (right) wind in latitude-altitude frame during vernal equinox are illustrated in figure 7, and similar plot of semi-diurnal component is shown in figure 8. The tidal response is plotted up to 100 km altitude and covers the latitude from 70°S to 70°N. The tidal response has hemispheric symmetry in general; although diurnal component is slightly stronger in the northern hemisphere. The diurnal tide peaks around ±20° to 25° latitude and minimizes towards the equator and poles, whereas, semi-diurnal tide is stronger at higher latitudes. This result is consistent with globally coordinated observations of winds in the mesosphere and lower thermosphere compiled by Deng *et al.* (1997). Semi-diurnal zonal tide shows symmetry at the equator with peaks at ±60° latitude. The semi-diurnal tide is weaker over the equator, and the amplitude diminishes rapidly at lower altitudes. The semi-diurnal tide is weaker for about an order of magnitude than the diurnal tide. The vertical wavelength for diurnal tide is about 22 km, whereas that of semi-diurnal

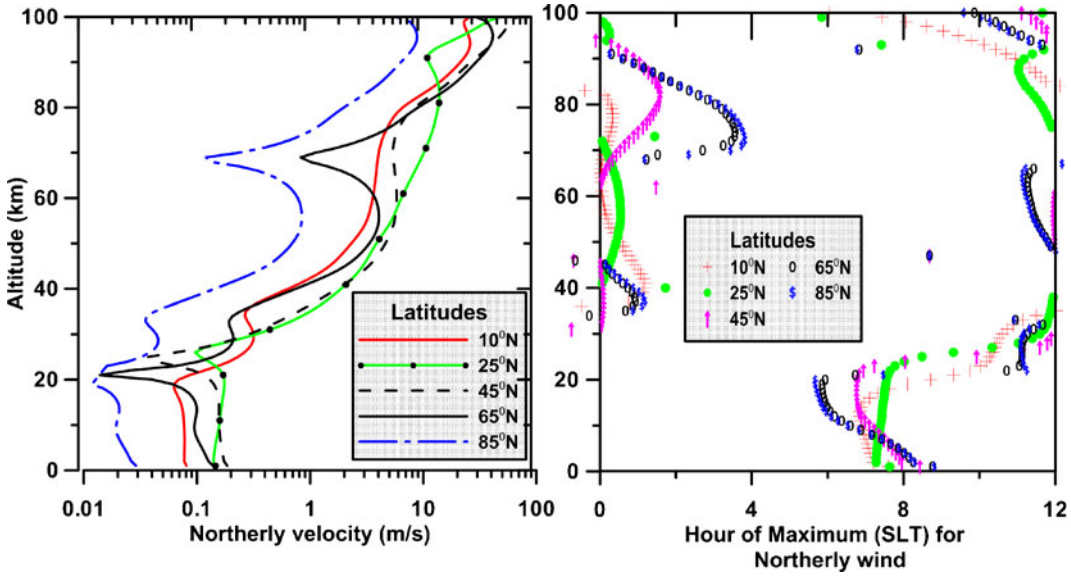

Figure 6. Same as figure 5, but for semi-diurnal component.

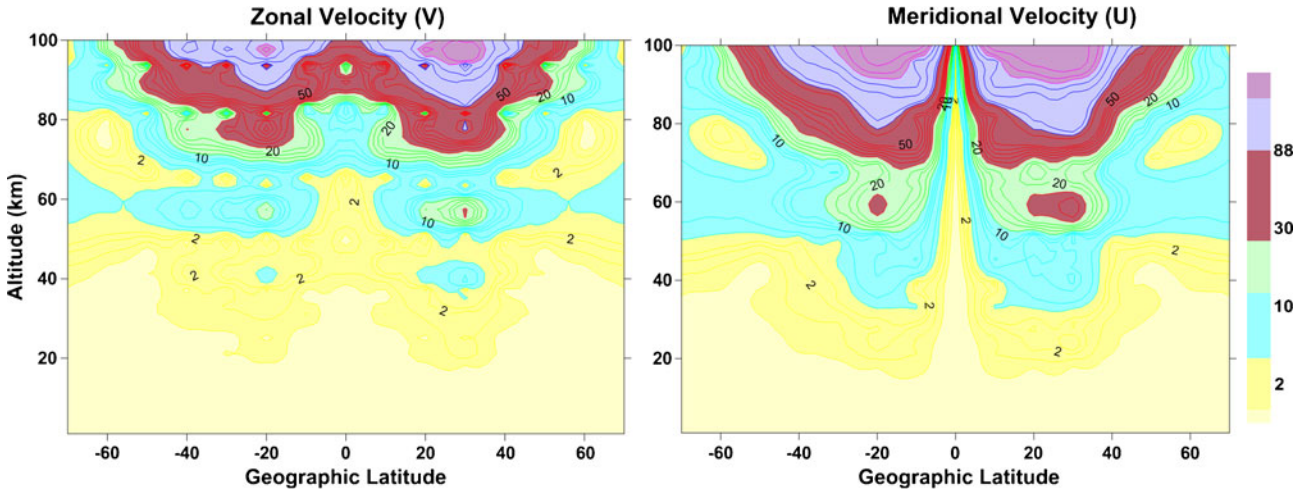

Figure 7. Contour plots of diurnal component of zonal (left) and meridional (right) tidal perturbations during March equinox as a function of altitude and latitude. Units of velocities are in m/s.

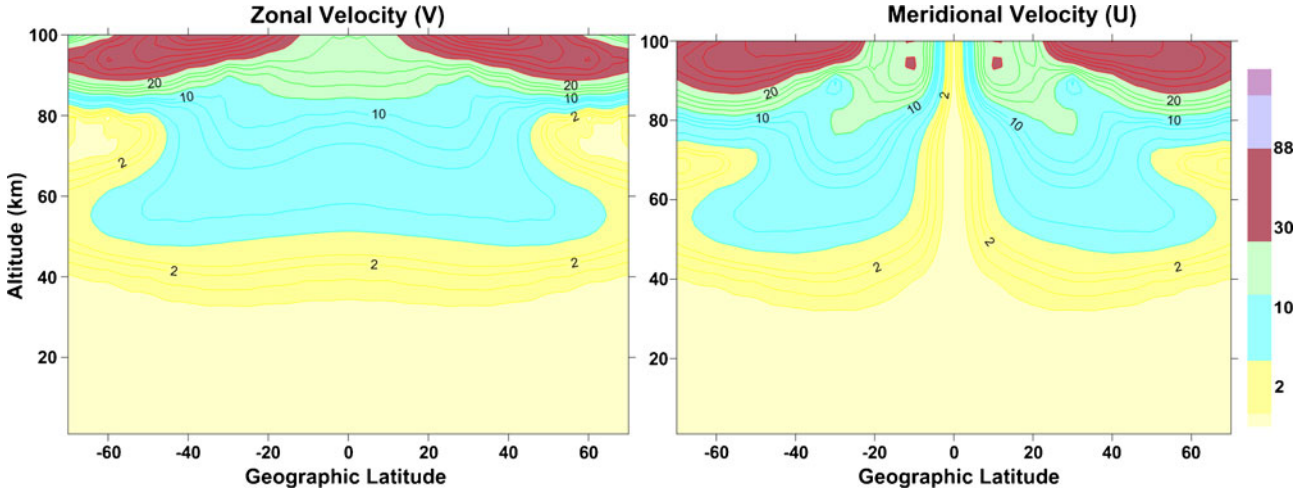

Figure 8. Same as figure 7, but for semi-diurnal component.

wave at higher latitudes is around 45–50 km, indicating longer vertical wavelength for semi-diurnal tide than diurnal tide. All these characteristic features are in good agreement with other sophisticated models such as GSWM. Moreover, a minimum seen in the diurnal zonal wind at ∼90 km over the equator seems to be consistent with the observations by Gurubaran and Rajaram (1999), who examined the variability of the mesospheric diurnal wind observed by medium frequency (MF) radar over equatorial station Tirunelveli, and found the amplitudes in general, tend to show a minimum around 92 km and an increase with altitude above.

Figure 9 illustrates the contour plot of vertical velocity, which is also symmetric at the equator. At 100 km altitude, the primary peak in diurnal component of vertical wind is observed over the equator, and the secondary peaks are seen around ±35° latitude. Semi-diurnal tide in the vertical velocity also peaks over the equator. Note that the magnitude of vertical wind is very small compared to other two components of wind and hence normally it is neglected.

Comparison of the contour plots of various components of wind obtained by present model with those computed by latest versions of GSWM (such as GSWM00, GSWM02) reveals very good qualitative match. The diurnal component of zonal and meridional winds using GSWM00 show peaks near ±25° latitude, which is consistent with present simulations. Also the features of vertical wind in GSWM match well with present results. Thus, although present model do not consider background wind and dissipative forces taking place in the atmosphere such as turbulence, diffusion of

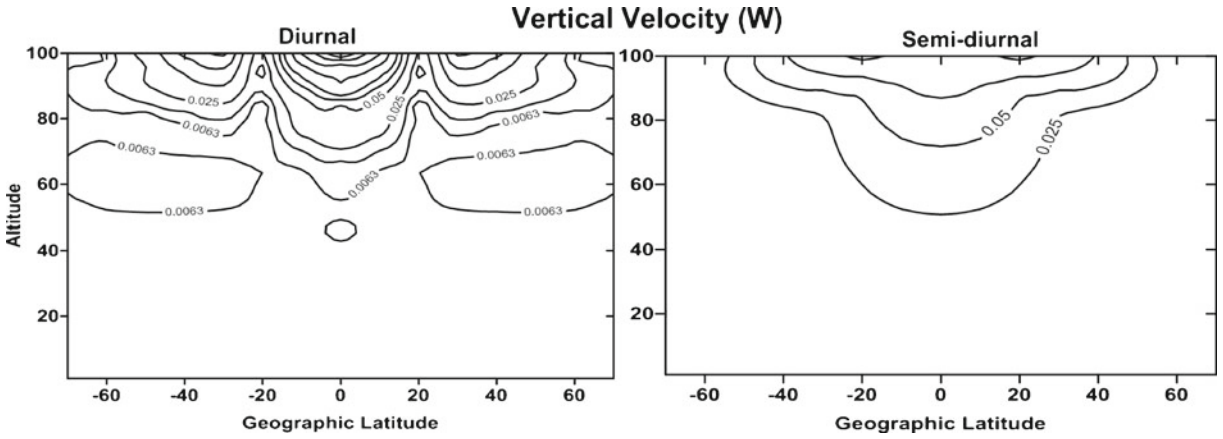

Figure 9. Contour plot of vertical velocity: (**a**) diurnal and (**b**) semi-diurnal component. Magnitude of the vertical velocity (m/s) is mentioned on the contours.

heat, infrared cooling, ion drag, etc., the salient features of the diurnal and semi-diurnal tidal responses are qualitatively unaffected.

6. Limitations of the present study and further issues

The complete strategy for the atmospheric thermal tidal computation can be split up into four components, viz., determination of thermal forcing, background medium, damping and method to solve the tidal equation. Present simulations assume zonally symmetric distribution of heating and hence study only the migrating part of the tides. We have already discussed about various sources of thermal excitation up to lower thermosphere in first section, which assumes longitudinal symmetry. However, other than those, there are some zonally non-symmetric heating drivers such as latent heat release in water vapour, outgoing long wave radiation (OLR), etc., which give non-migrating tides. Non-migrating tidal components are also harmonics of a solar day, but unlike migrating tides, their zonal wavenumber is not equal to frequency. This means that they may be stationary, or propagate either eastward or westward.

The background wind essentially flows due to the differences in the net global heating between the northern and southern hemispheres. The small-scale waves (such as gravity waves) are sufficiently large above 80 km to cause turbulence by accelerating the background air, which results in the eddy currents, that disrupts the tidal propagation. In the lower thermosphere, the decreasing density of the air causes wave motion to be dominated by molecular diffusion rather than fluid flow, which decreases the efficiency of energy transfer, and hence dampens the tides. The present model do not account for any such damping mechanism nor background winds. Hence, it is needed to modify the present set-up to include damping of the tides and mean background winds.

It should be noted that the prediction by existing sophisticated models differ from the actual observations, e.g., the observed amplitudes obtained from CRISTA 1 mission (Ward *et al.* 1999) are less than GSWM predictions. In general, the comparison of GSWM with climatological observations report good agreement for diurnal tides, while not good agreement for semi-diurnal tides (Palo *et al.* 1997; Vincent *et al.* 1998; Zhao *et al.* 2012). Similarly, study by Morel *et al.* (2004) has shown that the results with the inclusion of latest background wind model are not adequate to reproduce the observations and hence reported a need of more realistic background winds.

Therefore, other than the requisitions of background wind and dissipative forces, there is a need to invoke more realistic background atmosphere and heating sources in the model. The improvements related to heating sources can be sought through refinement of PHODIS model. Since the heating rates calculated by PHODIS model depend on the background atmosphere used, it would be appropriate to use most recent and realistic profile of the background atmosphere. Furthermore, elastic and inelastic collisions among electrons, ions and neutrals can also heat up the atmosphere. Also, auroral electrons, Joule dissipation of ionospheric currents can produce significant heating in the atmosphere. Thus, the scenario is nevertheless quite complicated as one proceeds to look for more realistic situation. However, some efforts are required in this direction in order to model the thermospheric heating more reasonably. Also, the model should inherently consider the variation of background environment with respect to latitudinal sectors, seasons and solar activity. Similarly, clouds, i.e., increased quantity of H_2O would have

an appreciable effect on the tidal structures. During low latitude monsoon season, the relative sensitivity of the tides to such excitation, need to be recognized while comparing model results with the observations. Further, the future version of PHODIS may further improve parameterization for the computation of heating rates and can be used for future tidal evaluation.

7. Summary

The main aim of the present study is to compute the tidal structures due to conventional ozone and water vapour heating along with the heating due to absorption by molecular oxygen. The PHODIS, radiative transfer model is capable of providing heating rates due to combined effect of solar and chemical heating in the wavelength region 116 to 850 nm. The present atmospheric tidal model based on PHODIS heating and tropospheric water vapour absorption reveals following features of the diurnal and semi-diurnal tides. The diurnal amplitude peaks in mid-to-low latitudes, whereas semi-diurnal component is stronger at higher latitudes. The semi-diurnal tide is weaker for about an order of magnitude than the diurnal tide. Similarly, semi-diurnal wave has longer wavelength than diurnal tide. The features of the tidal structures obtained here are in qualitative agreement with GSWM output (Hagan 1996), thus proves the validity of the present model. However, the magnitudes of the winds obtained in the present simulation are higher than GSWM results. This may suggest that the background wind profile and dissipation mechanisms essentially play a role in controlling the strength of the tides, rather than affecting the qualitative structure of it. Section 6 has discussed the scope for further improvement of the model. Other than the issues of dissipation and mean wind, there are few more concerns which need to be addressed such as thermospheric heating due to charged particles, presence of clouds, non-migrating tides, etc.

The program and the method of solution adopted here are arranged in such a way that it can perform tidal computations for any mode, e.g., two-wave, planetary scale waves, etc., and hence one can examine the patterns of various tidal modes. The flexibility of present model for different parameters involved such as temperature, pressure, different tidal modes, etc., would facilitate to study day-to-day variability of the tidal components. Moreover, the computational requirement for running the code is minimum, and hence the present model can be considered as most economical. Therefore it can emerge as a better substitute for presently available tidal models.

Acknowledgement

The authors are thankful to Arve Kylling for making available PHODIS package through anonymous ftp to kaja.gi.alaska.edu/pub/arve.

References

Anderson G P, Clough S A, Kneizys F X, Chetwynd J H and Shettle E P 1986 AFGL Atmospheric Constituent Profiles (0–120 km); Air Force Geophysics Laboratory Report AFGL-TR-86-0-10, Environmental Research Paper No. 954, May 1986.

Butler S T and Small K A 1963 The Excitation of Atmospheric Oscillations; *Proc. Roy. Soc. London A* **274** 91–121, doi: 10.1098/rspa.1963.0116.

Chapman S and Lindzen R S 1970 *Atmospheric Tides*; Dordrecht: Reidel Publications.

Dahlback A and Stamnes K 1991 A new spherical model for computing the radiation field available for photolysis and heating at twilight; *Planet. Space Sci.* **39** 671–683.

Damski J, Tholix L, Backman L, Kaurola J, Taalas P, Austin J, Butchart N and Kulmala M 2007 A chemistry-transport model simulation of middle atmospheric ozone from 1980 to 2019 using coupled chemistry GCM winds and temperatures; *Atmos. Chem. Phys. Discuss.* **7** 1143–1181.

DeMore W B, Howard C J, Sander S P, Ravishankara A R, Golden D M, Kolb C E, Hampson R F, Molina M J and Kurylo M J 1992 Chemical kinetics and photochemical data for use in stratospheric modeling; JPL Publ. 92–20, Jet Propulsion Lab., Pasadena, Calif.

Deng W *et al.* 1997 Coordinated global radar observations of tidal and planetary waves in the mesosphere and lower thermosphere during January 20–30 1993; *J. Geophys. Res.* **102(A4)** 7307–7318.

Forbes J M 1982 Atmospheric tides I, model description and results for the solar diurnal component; *J. Geophys. Res.* **87** 5222–5240.

Forbes J M and Garrett H B 1978 Thermal excitation of atmospheric tides due to insolation absorption of O_3 and H_2O; *Geophys. Res. Lett.* **5** 1013–1016.

Grieger N, Volodin E N, Schmitz G, Hoffmann P, Manson A, Fritts D, Igarashi K and Singer W 2002 General circulation model results on migrating and nonmigrating tides in the mesosphere and lower thermosphere. Part I: Comparison with observations; *J. Atmos. Sol.-Terr. Phys.* **64** 897–911.

Groves G B 1982 Hough components of water vapor heating; *J. Atmos. Terr. Phys.* **44** 281–290.

Groves G V and Wilson A 1982 Diurnal, semi-diurnal and terdiurnal Hough components of surface pressure; *J. Atmos. Terr. Phys.* **44** 599–611.

Gurubaran S and Rajaram R 1999 Long-term variability in the mesospheric tidal winds observed by M F radar over Tirunelveli (8.7°N, 77.8°E); *Geophys. Res. Lett.* **26(8)** 1113–1116.

Hagan M E 1996 Comparative effects of migrating solar sources on tidal signatures in the middle and upper atmosphere; *J. Geophys. Res.* **101(D16)** 21,213–21,222.

Hagan M E and Forbes J M 2002 Migrating and nonmigrating diurnal tides in the middle and upper atmosphere excited by tropospheric latent heat release; *J. Geophys. Res.* **107(D24)** 4754, doi: 10.1029/2001JD001236.

Hagan M E and Forbes J M 2003 Migrating and nonmigrating semidiurnal tides in the upper atmosphere excited

by tropospheric latent heat release; *J. Geophys. Res.* **108(A2)** 1062, doi: 10.1029/2002JA009466.

Jadhav Geeta 2002 *Theoretical modeling of low latitude current system*, Thesis, Mumbai University.

Kylling A, Stamnes K and Tsay S-C 1995 A reliable and efficient two-stream algorithm for spherical radiative transfer: Documentation of accuracy in realistic layered media; *J. Atmos. Chem.* **21** 115–150.

Lieberman R S and Leovy C B 1995 A numerical model of nonmigrating diurnal tides between the surface and 65 km; *J. Atmos. Sci.* **52(4)** 389–409.

Minschwaner K, Salawitch R J and McElroy M B 1993 Absorption of solar radiation by O_2: Implications for O_3 and lifetimes of N_2O, $CFCl_3$, and CF_2Cl_2; *J. Geophys. Res.* **98(D6)** 0148–0227.

Miyahara S and Miyoshi Y 1997 Migrating and nonmigrating atmospheric tides simulated by a middle atmosphere general circulation model; *Adv. Space Res.* **20** 1201–1207.

Mlynczak M G and Solomon S 1993 A detailed evaluation of the heating efficiency in the middle atmosphere; *J. Geophys. Res.* **98(D6)** 10,517–10,541, doi: 10.1029/93JD00315.

Molina L T and Molina M J 1986 Absolute absorption cross sections of ozone in the 185–350 nm wavelength range; *J. Geophys. Res.* **91** 14,501–14,508.

Morel B, Keckhut P, Bencherif H, Hauchecorne A, Megie G and Baldy S 2004 Investigation of the tidal variations in a 3D dynamics-chemistry-transport model of the middle atmosphere; *J. Atmos. Sol.-Terr. Phys.* **66** 251–265.

Nicolet M 1984 On the molecular scattering in the terrestrial atmosphere: An empirical formula for its calculation in the homosphere; *Planet. Space Sci.* **32** 1467–1468.

Palo S E, Hagan M E, Meek C E, Vincent R A, Burrage M D, McLandress C, Franke S J, Ward W E, Clark R R, Hoffmann P, Johnson R, KuÈrschner D, Manson A H, Murphy D, Nakamura T, Portnyagin YU I, Salah J E, Schminder R, Singer W, Tsuda T, Virdi T S and Zhou Q 1997 An intercomparison between the GSWM, UARS, and ground-based radar observations: A case-study in January 1993; *Ann. Geophys.* **15** 1123–1141.

Pancheva D, Mitchell N, Middleton H and Muller H 2003 Variability of the semidiurnal tide due to fluctuations in solar activity and total ozone; *J. Atmos. Sol.-Terr. Phys.* **65** 1–19.

Rajaram R and Gurubaran S 1998 Seasonal variabilities of low-latitude mesospheric winds; *Ann. Geophys.* **16** 197–204.

Ratnam M V, Narayana Rao D, Krishnaiah M, Bhavani Kumar Y, Siva Kumar V and Rao P B 2002 Coordinated MST radar and lidar observations for the study of mesospheric structures over a tropical station; *J. Atmos. Sol.-Terr. Phys.* **64** 349–358.

Reed R J, Oard M J and Sieminski Marya 1969 A comparison of observed and theoretical diurnal tidal motions between 30 and 60 km; *Mon. Weather Rev.* **97** 456–459.

Riggin D M, Meyer C K, Fritts D C, Jarvis M J, Murayama Y, Singer W, Vincent R A and Murphy D J 2003 MF radar observations of seasonal variability of semidiurnal motions in the mesosphere at high northern and southern latitudes; *J. Atmos. Sol.-Terr. Phys.* **65** 483–493.

Sasi M N and Krishna Murthy B V 1990 Diurnal and semidiurnal tides in the middle atmosphere over Balasore (21.5°N, 86.9°E); *J. Atmos. Sci.* **47(17)** 2101–2107.

Siebert M 1961 Atmospheric tides; *Adv. Geophys.* (New York: Academic Press) **7** 105–182.

Simpson W R, King M D, Beine H J, Honrath R E and Peterson M C 2002 Atmospheric photolysis rate coefficients during the Polar Sunrise Experiment ALERT2000; *Atmos. Environ.* **36** 2471–2480.

Simpson D, Benedictow A, Berge H, Bergstrom R, Emberson L D, Fagerli H, Hayman G D, Gauss M, Jonson J E, Jenkin M E, Nyiri A, Richter C, Semeena V S, Tsyro S, Tuovinen J P, Valdebenito A and Wind P 2012 The EMEP MSC-W chemical transport model – Part 1: Model description; *Atmos. Chem. Phys. Discuss.* **12** 3781–3874.

Stamnes K, Tsay S-C, Wiscombe W and Jayaweera K 1988 Numerically stable algorithm for discrete-ordinate-method radiative transfer in multiple scattering and emitting layered media; *Appl. Optics* **27** 2502.

Strobel D F 1978 Parameterization of the atmospheric heating rate from 15 to 120 km due to O_2 and O_3 absorption of solar radiation; *J. Geophys. Res.* **83** 6225–6230.

Tsuda T, Ohnishi K, Isoda F, Nakamura T, Vincent R, Reid I, Sri Woro B Harijono, Sribimawati T, Nuryanto A and Wiryosumart H 1999 Coordinated radar observations of atmospheric diurnal tides in equatorial regions; *Earth Planets Space* **51** 579–592.

Vincent R A 1984 MF/HF radar measurements of the dynamics of the mesosphere region – A review; *J. Atmos. Terr. Phys.* **46** 961–974.

Vincent R A, Kovalam S, Fritts D C and Isler J R 1998 Long-term MF radar observations of solar tides in the low-latitude mesosphere: Interannual variability and comparisons with the GSWM; *J. Geophys. Res.* **103(D8)** 8667–8683, doi: 10.1029/98JD00482.

Ward W E, Oberheide J, Riese M, Preusse P and Offermann D 1999 Tidal signatures in temperature data from CRISTA 1 mission; *J. Geophys. Res.* **104(D13)**, doi: 10.1029/1998JD100109.

WMO 1986 WMO (World Meteorological Organization), Atmospheric Ozone 1985, Assessment of our understanding of the processes controlling its present distribution and changes, Rep. 16, Global ozone res. and Monit. Proj., Geneva, Switzerland.

Wood A R and Andrews D G 1997 A spectral model for simulation of tides in the middle atmosphere. I: Formulation; *J. Atmos. Sol.-Terr. Phys.* **59** 31–51.

Xu J, Smith A K, Liu H-L, Yuan W, Wu Q, Jiang G, Mlynczak M G, Russell III J M and Franke S J 2009 Seasonal and quasi-biennial variations in the migrating diurnal tide observed by thermosphere, ionosphere, mesosphere, energetics and dynamics (TIMED); *J. Geophys. Res.* **114(D13107)**, doi: 10.1029/2008JD011298.

Zhang X, Forbes J M and Hagan M E 2010 Longitudinal variation of tides in the MLT region: 1. Tides driven by tropospheric net radiative heating; *J. Geophys. Res.* **115(A06316)**, doi: 10.1029/2009JA014897.

Zhao Lei, Jinsong Chen, Zonghua Ding, Na Li and Zhenwei Zhao 2012 First observations of tidal oscillations by an MF radar over Kunming (25.61N, 103.81E); *J. Atmos. Sol.-Terr. Phys.* **78–79** 44–52.

MS received 6 September 2012; revised 2 March 2013; accepted 27 March 2013